Dielectric Ring-Gap Resonator for Application in MMIC's

Wei Ke Hui and Ingo Wolff, *Fellow, IEEE*

Abstract—**A new dielectric resonator—the dielectric ring-gap resonator—is introduced and analyzed. The dielectric ring-gap resonator is obtained by sawing a narrow gap into a dielectric ring resonator. Resonant frequencies and unloaded Q factors of quasi-TE_{0pq} modes in the ring-gap resonator have been calculated by an appropriate equivalent circuit starting from the resonant frequencies and the field distributions of the TE_{0pq} modes in the ring resonator. The calculated resonant frequencies of the fundamental quasi-TE_{011} mode show an accuracy of $< 1\%$ compared with the experimental results. New coupling techniques to couple the ring-gap resonator to e.g. a microstrip line on a thin substrate, using the electric fringing field near the gap, have been experimentally investigated. A new rigorous method of determining resonant frequencies and field distributions of TE modes in a multicomposite multilayered cylindrical dielectric resonator is presented. This resonator consists of numbers of cylinders, which are arbitrarily layered in axial direction.**

I. Introduction

IT IS well known that dielectric resonators have not only the advantages of a small size and a small weight, but also these of a high unloaded Q factor and a high temperature stability of resonant frequencies [1]. They have brought significant improvement in the design of microwave oscillators [2] and filters [3]. Often used structures of the dielectric resonators are dielectric disc and ring resonators. In this article a new dielectric resonator —the dielectric ring-gap resonator—is introduced and analyzed. The dielectric ring-gap resonator is obtained by sawing a very narrow vertical gap (or slit) into a dielectric ring resonator. Its configuration and the field pattern of the fundamental quasi-TE_{011} mode are shown in Fig. 1.

The desired, technically applicable resonant mode in the dielectric ring-gap resonator has a similar field distribution to the TE_{011} mode in the corresponding dielectric ring resonator except the fringing fields in the vicinity of the gap and the electric field in the air gap, as shown in Fig. 1. This mode will be named quasi-TE_{011} mode. When the gap is sufficiently narrow, the magnetic fringing field near the gap is very weak and can be neglected. The electric fringing field near the gap edges can be much stronger than the electric field anywhere else outside the ring. The electric field in the air gap is ϵ_r times (ϵ_r is the relatively permittivity of the ring material) stronger than that in the dielectric ring.

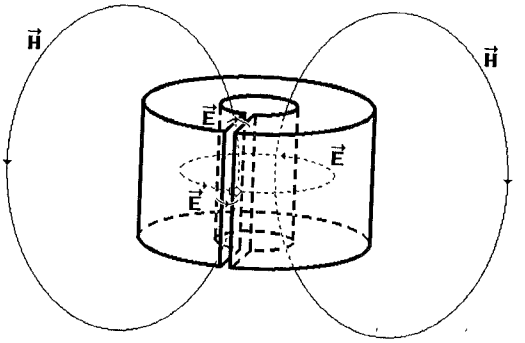

Fig. 1. Dielectric ring-gap resonator and the field pattern of the fundamental quasi-TE_{011} mode.

Besides the advantages of dielectric disc and ring resonators, the dielectric ring-gap resonator has four following important properties:

1) If the gap in the dielectric ring resonator is sufficiently small, some lower order TE_{0pq} modes of the ring resonator are disturbed by the gap only in the vicinity of the gap and the resonant frequencies of the modes are raised a little. They will be named quasi-TE_{0pq} modes. Furthermore the fundamental quasi-TE_{011} mode can be excited effectively suppressing other undesired higher order modes at the same time. The best experimental result shows that the desired fundamental mode can be excited dominantly over a measured frequency range from 45 MHz to 40 GHz in a proper designed ring-gap resonator.

2) The dielectric ring-gap resonator may be coupled directly to a microstrip line, to a slotline or to a coplanar waveguide on a MMIC chip by the electric fringing field near the gap edges.

3) The resonant frequency of the dielectric ring-gap resonator can be tuned by a dielectric slice in the gap besides the tuning techniques used in the dielectric ring resonator.

4) The dielectric ring-gap resonator has a higher dielectric Q factor due to some of the electric field energy stored in the lossless air gap, but a lower conductor Q factor than the dielectric ring resonator. The total Q factor may be higher or lower compared to the ring resonator dependent on the geometrical structure.

Manuscript received March 15, 1991; revised July 10, 1991.

The authors are with the Department of Electrical Engineering and Sonderforschungsbereich Duisburg University, FB 9/ATE, Bismarckstr 81, 4100 Duisburg 1, Germany.

IEEE Log Number 9102778.

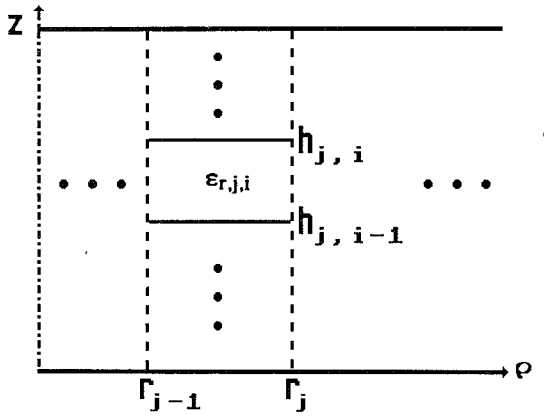

Fig. 2. Multicomposite multilayered cylindrical dielectric resonator structure.

In 1981, a rigorious analysis method based on the mode matching technique to determine resonant frequencies and field distributions of various modes in a shielded dielectric ring and rod resonator was first introduced [4], [5]. Later, this method was developed to study a composite multilayered cylindrical dielectric resonator [6], [7], which is composed of two or three concentric cylinders filled with different dielectric layers in axial direction. In this paper, it is further extended to study TE modes in a more generalized dielectric resonator. This resonator consists of a number of concentric cylinders, which are arbitrarily layered in axial direction, and will be named multicomposite multilayered cylindrical dielectric resonator, as shown in Fig. 2.

II. Theoretical Analysis

A. Quasi-TE_{0pq} Modes in the Dielectric Ring-Gap Resonator

A dielectric ring-gap resonator structure used in practice is usually composed of a dielectric ring-gap sample and some dielectric concentric cylinders or plates, which are together placed between two parallel conducting plates perpendicular to the sample axis or concentrically enclosed in a cylindrical conducting cavity. For example, Fig. 3 shows a dielectric ring-gap resonator composed of a ring-gap sample, a substrate and a tubular dielectric spacer together placed between two parallel conducting plates. In the following analysis, it is assumed that a generalized dielectric ring-gap resonator consists of N ($N = 4$ in Fig. 3) different dielectric materials enclosed in a metal shield. ϵ_{rn} and $\tan\delta_{dn}$ represent the relative permittivity and the loss tangent of each dielectric material, respectively. R_s represents the surface resistance of the metal shield. The material "1" is the ring-gap sample and has a much higher relative permittivity than the others. The sample cut by a vertical slot (or gap) has a fan-shaped horizontal section, whose two radial sides divide the space of the resonator into two volumes V_g and V_r as shown in Fig. 3. V_g represents the small wedge-shaped slot volume included the gap and V_r is another part of the resonator. φ_s is the circular angle of the gap in radian and s is the average gap distance.

Though a ring-gap resonator can be considered as a ring resonator cut by a vertical gap in the ring sample, the field distributions of various resonant modes in the ring-gap resonator cannot directly be derived from those in the ring resonator. This is due to the fact that an influence of the gap on the field distributions of the ring resonator is strongly dependent on the gap size and the field structure of various modes. For a sufficiently small gap and some modes, e.g., some lower order TE modes, the field distributions in the ring resonator are distorted only in the vicinity of the gap. They will be named quasi-TE_{0pq} modes. The quasi-TE_{0pq} mode in the ring-gap resonator has similar field distributions to the TE_{0pq} mode in the ring resonator except the electric field in the air gap and the fringing fields in the vicinity of the gap. The magnetic fringing field near the gap is very weak and can be neglected. The electric fringing field near the gap edges can be much stronger than the electric field anywhere else outside the sample. The electric field in the air gap is ϵ_{r1} times stronger than that in the dielectric part of the sample.

Therefore, the field distributions of the quasi-TE_{0pq} modes in the ring-gap resonator to a first approximation can be described by those of the TE_{0pq} modes in the ring resonator except the gap fringing fields.

Fig. 4(a) shows an appropriate equivalent circuit for each quasi-TE_{0pq} mode in the dielectric ring-gap resonator and its simplified circuit in Fig. 4(b). The equivalent circuit (Fig. 4(a)) is composed of an inductor L_r, whose value is equal to that for the case of the ring resonator, and two parallel RC circuits. One of the RC circuits ($C_{rg,r}$, $R_{d,rg,r}$ and $R_{c,rg,r}$) is used to characterize the stored electric energy and the dissipated power, leaded by dielectric and conductor losses respectively, in the volume V_r of the resonator outside the slot region (Fig. 3). Another ($C_{rg,g}$, C_f, $R_{d,rg,g}$ and $R_{c,rg,g}$) characterizes those in the small slot volume V_g. C_f is an equivalent additional capacitance due to existence of the electric fringing field near the gap. The equivalent circuit in Fig. 4(a) can be derived from that for the TE_{0pq} mode of the corresponding ring resonator under following assumptions:

1) Magnetic induced currents I_r through any longitudinal section of ring-gap resonator are equal, because of neglecting the magnetic fringing field of the quasi-TE_{0pq} mode.

2) An additional inductance and an additional conductor loss resistance, leaded by existence of the magnetic fringing field, can be neglected.

3) An additional dielectric loss resistance by the electric fringing field can be neglected, because most of the electric fringing field is distributed in lossless air spaces.

4) The equivalent fringing capacitance C_f should be much smaller than the capacitance $C_{rg,g}$ of the slot volume V_g.

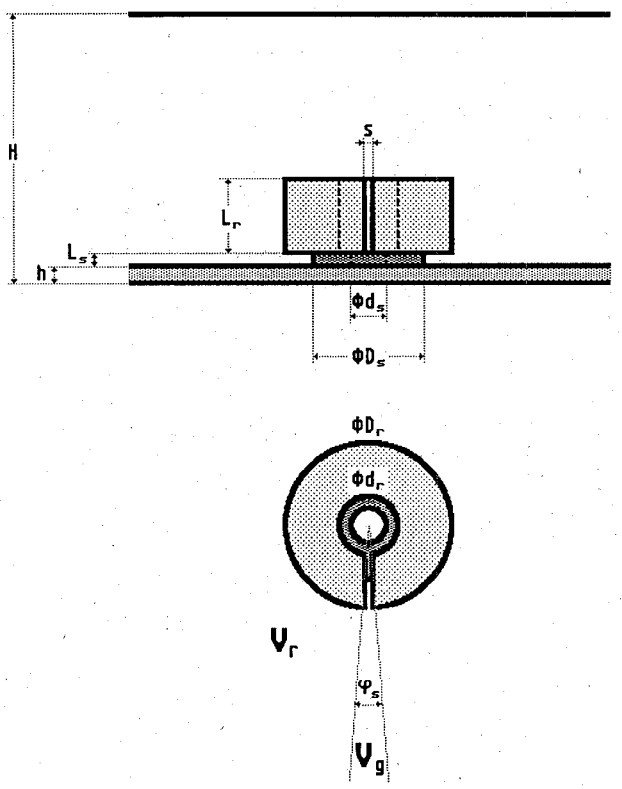

Fig. 3. Shielded dielectric ring-gap resonator structure.

All equivalent capacitances except C_f and resistances can be derived from those of the ring resonator and are presented by

$$C_{rg,r}=\frac{2\pi}{\varphi_r}C_r,\quad R_{d,rg,r}=\frac{\varphi_r}{2\pi}R_d,$$

$$R_{c,rg,r}=\frac{\varphi_r}{2\pi}R_c,$$

$$C_{rg,g}=\frac{2\pi}{\varphi_s}\left(\frac{C_{r1}}{\epsilon_{r1}}+\sum_{n=2}^{N}C_{rn}\right),$$

$$R_{d,rg,g}=1\Big/\left(\frac{2\pi}{\varphi_s}\sum_{n=2}^{N}\frac{1}{R_{dn}}\right),\qquad R_{c,rg,g}=\frac{\varphi_s}{2\pi}R_c,$$

$$R_{d,rg}=\left(\frac{C_{rg,r}+C_{rg,g}}{C_{rg,g}}\right)^2 R_{d,rg,r}+\left(\frac{C_{rg,r}+C_{rg,g}}{C_{rg,r}}\right)^2 R_{d,rg,g},$$

$$R_{c,rg}=\left(\frac{C_{rg,r}+C_{rg,g}}{C_{rg,g}}\right)^2 R_{c,rg,r}+\left(\frac{C_{rg,r}+C_{rg,g}}{C_{rg,r}}\right)^2 R_{c,rg,g},\tag{1}$$

where φ_s is the circular angle of the gap in radian as shown in Fig. 3, $\varphi_r=2\pi-\varphi_s$. All equivalent elements of

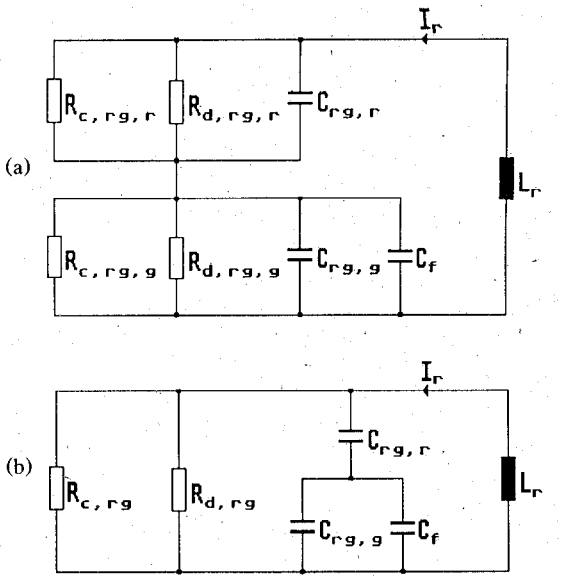

Fig. 4. (a) Equivalent circuit for the quasi-TE_{0pq} mode in the dielectric ring-gap resonator. (b) Simplified circuit of Fig. 4(a).

the ring resonator can be expressed by

$$L_r=\frac{4W_e}{I_r^2},\qquad C_r=\sum_{n=1}^{N}C_{rn},\qquad R_d=1\Big/\sum_{n=1}^{N}\frac{1}{R_{dn}},$$

$$R_c=\frac{8\omega_r^2W_e^2}{I_r^2P_c},$$

with

$$W_e=\sum_{n=1}^{N}W_{en},\qquad C_{rn}=\frac{I_r^2W_{en}}{4\omega_r^2W_e^2},\qquad R_{dn}=\frac{8\omega_r^2W_e^2}{I_r^2P_{dn}},\tag{2}$$

where ω_r is the resonant angular frequency of the ring resonator. W_{en} and P_{dn} represent the stored electric energy and the dissipated power in each dielectric material, respectively. P_c represents the dissipated power in the conducting shield and I_r is the total current through any longitudinal section of the resonator. They can be obtained by integrating the field distributions of the considered TE_{0pq} mode:

$$W_{en}=\frac{1}{4}\epsilon_0\epsilon_{rn}\iiint_{V_{dn}}|E_\varphi|^2\,dv,\qquad P_{dn}=W_{en}\tan\delta_{dn},$$

$$P_c=\frac{1}{2}R_s\iint_{A_c}|\vec{H}|^2\,dA,\qquad I_r=\int_{C_z}|H_z(\rho=0,z)|\,dz,\tag{3}$$

where V_{dn} represents the volume of each dielectric material, A_c the inner surface area of the metal shield and C_z the z-axis of the symmetry. The resonant frequencies and the field distributions of the TE_{0pq} modes in the dielectric ring resonator will be accurately determined by a rigorous analysis method (see following).

The resonant frequency and the unloaded Q factor, leaded by dielectric and conductor losses, of each quasi-TE_{0pq} mode in the dielectric ring-gap resonator can be evaluated by neglecting C_f in the equivalent circuits, because C_f is much smaller than $C_{rg,g}$.

In (1), the dielectric loss resistance $R_{d,rg,g}$ of the ring-gap resonator in the slot volume V_g can be very large, the conductor loss resistance $R_{c,rg,g}$ is equal to that for the case of the ring resonator, and the volume capacitance $C_{rg,g}$ is about ϵ_{r1} times smaller than that of the ring resonator. Therefore, the ring-gap resonator has a higher dielectric Q factor, but lower conductor Q factor than the ring resonator.

B. A Multicomposite Multilayered Cylindrical Dielectric Resonator

A multicomposite multilayered cylindrical dielectric resonator consists of numbers of concentric cylinders, which are arbitrarily layered in axial direction, as shown in Fig. 2. The resonator is divided into J complementary annular regions with radii of r_j $(j=1\sim J, r_0=0)$. Each partial region is filled with I_j different dielectric layers with heights of $h_{j,i}$ $(i=1\sim I_j,\ h_{j,0}=0,\ h_{j,I_j}=H)$. $\epsilon_{rj,i}$ represents the relative permittivity of the material of the ith layer in the jth region. It is assumed that all dielectric materials are lossless and the metal shield is perfectly conducting.

For the TE axial symmetric modes, the electric field has only one $E_\varphi(\rho,z)$-component and two magnetic field components $H_\rho(\rho,z)$ and $H_z(\rho,z)$ can be expressed by $E_\varphi(\rho,z)$. The electric field in each partial region can be represented in terms of a series of the TE modes in a dielectrically-loaded waveguide filled with I_j different dielectric layers $\{Z_{n,j}(z)\}$ by

$$E_\varphi(\rho,z)=\sum_{n=1}^{\infty} R_{n,j}(\rho)Z_{n,j}(z), \qquad (r_{j-1}\leqslant\rho\leqslant r_j), \quad (4)$$

where radial functions $\{R_{n,j}(\rho)\}$ and orthonormal eigenfunctions $\{Z_{n,j}(z)\}$ in each partial region are represented by

$$R_{n,j}(\rho)=R_{n,j}(r_{j-1})P_{n,j}(\rho)+R_{n,j}(r_j)Q_{n,j}(\rho), \quad (j=1\sim J,\ r_{j-1}\leqslant\rho\leqslant r_j), \quad (5)$$

$$Z_{n,j}(z)=Z_{n,j}(h_{j,i})F_{n,j,i}(z)+Z_{n,j}(h_{j,i-1})G_{n,j,i}(z), \quad (i=1\sim I_j,\ h_{j,i-1}\leqslant z\leqslant h_{j,i}), \quad (6)$$

where $P_{n,j}(\rho)$ and $Q_{n,j}(\rho)$ are given by linear combinations of appropriate cylinder functions, and $F_{n,j,i}(z)$ and $G_{n,j,i}(z)$ of trigonometric functions. In this paper, they are so selected that at the surfaces $\rho=r_{j-1}$, r_j and $z=h_{j,i-1}, h_{j,i}$ they are equal to 0 or 1:

$$\begin{array}{ll} F_{n,j,i}(z=h_{j,i-1})=0, & F_{n,j,i}(z=h_{j,i})=1,\\ G_{n,j,i}(z=h_{j,i-1})=1, & G_{n,j,i}(z=h_{j,i})=0,\\ P_{n,j}(\rho=r_{j-1})=1, & P_{n,j}(\rho=r_j)=0,\\ Q_{n,j}(\rho=r_{j-1})=0, & Q_{n,j}(\rho=r_j)=1, \end{array} \quad (7)$$

and presented by

$$F_{n,j,i}(z)=\sin\left[\beta_{n,j,i}(z-h_{j,i-1})\right]/\sin\left[\beta_{n,j,i}(h_{j,i}-h_{j,i-1})\right],$$
$$G_{n,j,i}(z)=\sin\left[\beta_{n,j,i}(h_{j,i}-z)\right]/\sin\left[\beta_{n,j,i}(h_{j,i}-h_{j,i-1})\right], \quad (8)$$

and

$$P_{n,j}(\rho)=\begin{cases}\dfrac{I_1(\alpha_{n,j}r_j)K_1(\alpha_{n,j}\rho)-K_1(\alpha_{n,j}r_j)I_1(\alpha_{n,j}\rho)}{I_1(\alpha_{n,j}r_j)K_1(\alpha_{n,j}r_{j-1})-K_1(\alpha_{n,j}r_j)I_1(\alpha_{n,j}r_{j-1})}, & \left(\alpha_{n,j}=\sqrt{\lambda_{n,j}},\ \lambda_{n,j}>0\right),\\ \dfrac{N_1(\gamma_{n,j}r_j)J_1(\gamma_{n,j}\rho)-J_1(\gamma_{n,j}r_j)N_1(\gamma_{n,j}\rho)}{N_1(\gamma_{n,j}r_j)J_1(\gamma_{n,j}r_{j-1})-J_1(\gamma_{n,j}r_j)N_1(\gamma_{n,j}r_{j-1})}, & \left(\gamma_{n,j}=\sqrt{-\lambda_{n,j}},\ \lambda_{n,j}<0\right),\end{cases}$$

$$\text{for } r_j\to\infty,\quad P_{n,j}(\rho)\begin{cases}K_1(\alpha_{n,j}\rho)/K_1(\alpha_{n,j}r_{j-1}), & \left(\alpha_{n,j}=\sqrt{\lambda_{n,j}},\ \lambda_{n,j}>0\right),\\ H_1^{(2)}(\gamma_{n,j}\rho)/H_1^{(2)}(\gamma_{n,j}r_{j-1}), & \left(\gamma_{n,j}=\sqrt{-\lambda_{n,j}},\ \lambda_{n,j}<0\right),\end{cases}$$

$$Q_{n,j}(\rho)=\begin{cases}\dfrac{I_1(\alpha_{n,j}\rho)K_1(\alpha_{n,j}r_{j-1})-K_1(\alpha_{n,j}\rho)I_1(\alpha_{n,j}r_{j-1})}{I_1(\alpha_{n,j}r_j)K_1(\alpha_{n,j}r_{j-1})-K_1(\alpha_{n,j}r_j)I_1(\alpha_{n,j}r_{j-1})}, & \left(\alpha_{n,j}=\sqrt{\lambda_{n,j}},\ \lambda_{n,j}>0\right),\\ \dfrac{N_1(\gamma_{n,j}\rho)J_1(\gamma_{n,j}r_{j-1})-J_1(\gamma_{n,j}\rho)N_1(\gamma_{n,j}r_{j-1})}{N_1(\gamma_{n,j}r_j)J_1(\gamma_{n,j}r_{j-1})-J_1(\gamma_{n,j}r_j)N_1(\gamma_{n,j}r_{j-1})}, & \left(\gamma_{n,j}=\sqrt{-\lambda_{n,j}},\ \lambda_{n,j}<0\right),\end{cases}$$

$$\text{for } r_{j-1}=0,\quad Q_{n,j}(\rho)=\begin{cases}I_1(\alpha_{n,j}\rho)/I_1(\alpha_{n,j}r_j), & \left(\alpha_{n,j}=\sqrt{\lambda_{n,j}},\ \lambda_{n,j}>0\right),\\ J_1(\gamma_{n,j}\rho)/J_1(\gamma_{n,j}r_j), & \left(\gamma_{n,j}=\sqrt{-\lambda_{n,j}},\ \lambda_{n,j}<0\right).\end{cases} \quad (9)$$

The unknown values $\beta_{n,j,i}$ in (8) and $\lambda_{n,j}$ in (9) have the relationship

$$\beta_{n,j,i}^2 = \lambda_{n,j} + (2\pi f_r)^2 \epsilon_0 \mu_0 \epsilon_{r,j,i}. \tag{10}$$

If the field components $E_\varphi(\rho, z)$ and $H_z(\rho, z)$ are "matched" at each surface of adjacent regions to satisfy the continuity condition, $2\times(J-1)$ equations are obtained in terms of the series $\{Z_{n,j}(z)\}$:

$$\sum_{n=1}^{\infty} R_{n,j}(r_j) Z_{n,j}(z) = \sum_{n=1}^{\infty} R_{n,j+1}(r_j) Z_{n,j+1}(z),$$

$$\sum_{n=1}^{\infty} \left\{ R_{n,j}(r_{j-1}) \hat{P}_{n,j}(r_j) + R_{n,j}(r_j) \hat{Q}_{n,j}(r_j) \right\} Z_{n,j}(z)$$

$$= \sum_{n=1}^{\infty} \left\{ R_{n,j+1}(r_j) \hat{P}_{n,j+1}(r_j) + R_{n,j+1}(r_{j+1}) \hat{Q}_{n,j+1}(r_j) \right\} Z_{n,j+1}(z),$$

$$(j = 1 \sim J-1), \tag{11}$$

with

$$\hat{P}_{n,j}(\rho) = \frac{1}{\rho} \frac{d}{d\rho} \{\rho P_{n,j}(\rho)\},$$

$$\hat{Q}_{n,j}(\rho) = \frac{1}{\rho} \frac{d}{d\rho} \{\rho Q_{n,j}(\rho)\}.$$

If the equations are "tested" with testing functions $\{Z_m(z)\}$, which are the TE modes in an air-loaded parallel-plate waveguide and can be presented by

$$Z_m(z) = \sqrt{\frac{2}{H}} \sin\left(\frac{m\pi z}{H}\right), \tag{12}$$

an infinite homogeneous system of simultaneous linear equations is obtained for the unknown expansion coefficients $R_{n,j}(r_{j-1})$ and $R_{n,j}(r_j)$ $(j = 1 \sim J,\ R_{n,1}(r_0 = 0) = R_{n,J}(r_J) = 0)$. This system has nontrivial solutions only if its determinant vanishes. Hence, the resonant frequencies of the TE_{0pq} modes can be found by searching for the zeros of the determinant. In practice, the system is truncated to a finite size of $\{2\times(J-1)\times N\}\times\{2\times(J-1)\times N\}$ (N is the number of the terms of the series (4)).

The above-mentioned numerical field analysis has four following advantages:

1) The method can be used to analyze a more complex structure of cylindrical dielectric resonators, because the orthogonal eigenfunctions $\{Z_{n,j}(z)\}$ can represent the TE modes in dielectrically-loaded waveguides, which are arbitrarily layered in axial direction, the testing functions $\{Z_m(z)\}$ are the air-loaded waveguide modes and the radial functions $\{R_{n,j}(\rho)\}$ are valid to all partial regions.

2) Fewer unknown coefficients $(Z_{n,j}(h_{j,i}),\ i = 1 \sim I_j - 1)$ are included in the orthonormal eigenfunctions $\{Z_{n,j}(z)\}$. Hence, an eigenvalue problem of a homogeneous system of $I_j - 1$ simultaneous linear equations with $I_j - 1$ unknown coefficients $Z_{n,j}(h_{j,i})$ $(i = 1 \sim I_j - 1)$ is solved for determining the eigenfunctions.

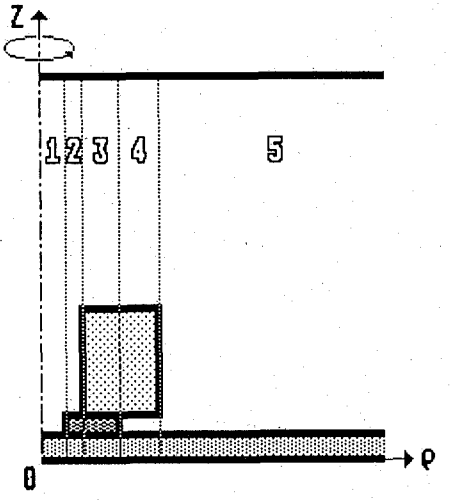

Fig. 5. Dielectric ring resonator structure.

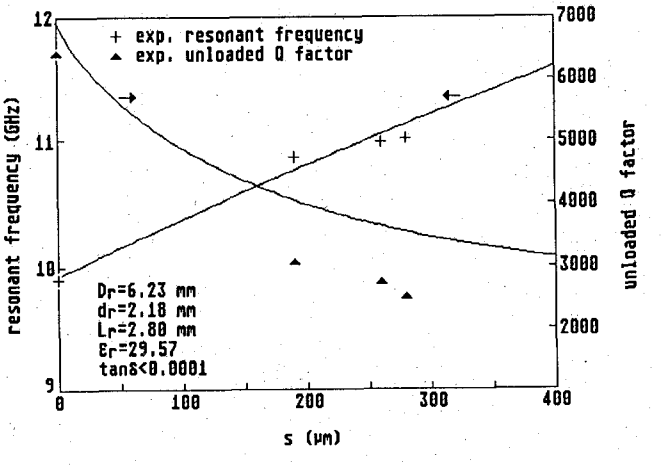

Fig. 6. Resonant frequencies and unloaded Q factors versus the gap size (s).

3) Contributions of nth TE mode in jth dielectrically-loaded waveguide to the electric field $E_\varphi(\rho, z)$ are directly connected to the unknown coefficients $R_{n,j}(r_{j-1})$, $R_{n,j}(r_j)$. Therefore, a more accurate result can be obtained by reducing the rounding error of the computer calculation.

4) This method can further be extended to analyze TM and hybrid modes in the multicomposite multilayered cylindrical dielectric resonators.

III. Numerical and Experimental Results

Some dielectric ring-gap resonators have been theoretically and experimentally investigated. They are composed of different dielectric ring-gap samples placed on a tubular dielectric spacer ($D_s = 4.14$ mm, $d_s = 1.3$ mm, $L_s = 0.50$ mm, $\epsilon_r = 4.45$) over a substrate ($h = 0.635$ mm, $\epsilon_r = 10$) and between two parallel conducting plates ($H = 10$ mm), as shown in Fig. 3. It is assumed that all dielectric materials have the same dielectric loss tangent of $\tan\delta_d = 0.0001$ and the metal enclosure has a conductivity of $\sigma = 2\cdot 10^5\ (\Omega\text{cm})^{-1}$. Because the dielectric ring-gap samples have different diameters from the tubular dielectric

TABLE I
COMPARISON OF CALCULATED AND EXPERIMENTAL RESULTS OF THE RESONANT FREQUENCIES (f_r) AND THE UNLOADED Q FACTORS (Q_r)

No.	D_r (mm)	d_r (mm)	L_r (mm)	ϵ_r	s (μm)	f_r (GHz) Theo.	f_r (GHz) Exp.	Q_r Theo.	Q_r Exp.
1	6.23	2.18	2.80	29.57	190	10.757	10.861	4030	3130
2	6.23	2.18	2.80	29.57	270	11.087	10.980	3600	2780
3	6.23	2.18	2.80	29.57	280	11.128	11.011	3550	2550
4	6.74	2.11	2.51	28.07	270	11.017	10.914	3330	2850

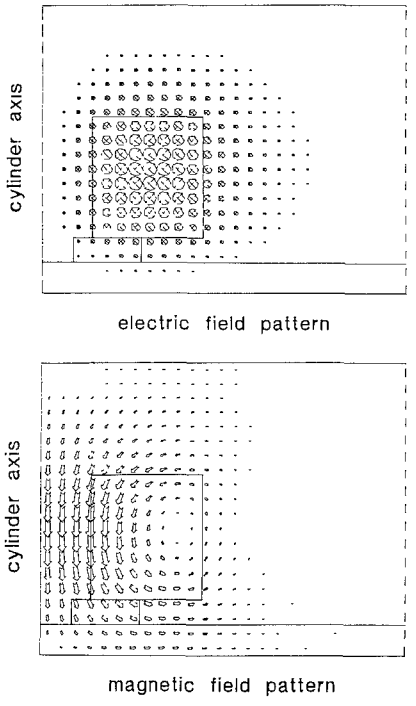

Fig. 7. Field pattern in a φ = const. plane of the TE_{011} mode of a dielectric ring resonator. Resonant frequency $f_r = 10.156$ GHz.

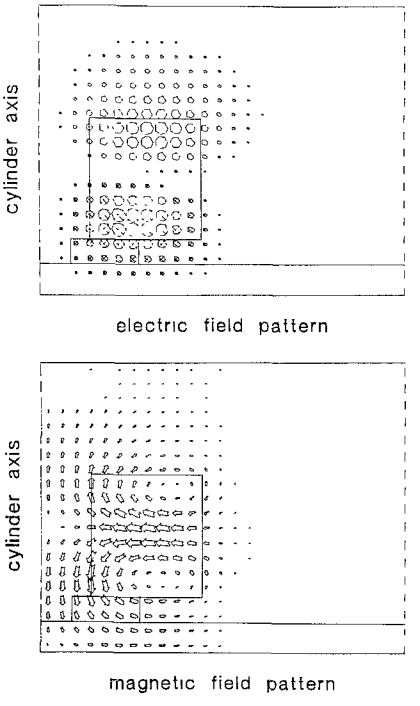

Fig. 8. Field pattern in a φ = const. plane of the TE_{012} mode of the resonator of Fig. 7. Resonant frequency $f_r = 17.444$ GHz.

spacer, the corresponding ring resonators must be divided into five complementary annular regions (Fig. 5), so that the permittivity ϵ_r in each region is independent on the radial coordinate ρ. They have theoretically been analyzed as multicomposite multilayered cylindrical dielectric resonators.

In Table I and in Fig. 6, the calculated values of resonant frequencies and unloaded Q factors of the fundamental quasi-TE_{011} mode for different ring-gap samples and for samples with different gap sizes (s), respectively, are compared with the experimental results. The calculated resonant frequencies show an accuracy of $< 1\%$ compared with the experimental results, though the fringing capacitance C_f and the additional inductance by magnetic fringing field are neglected. The error in Q factor calculations (Fig. 6) for the case of the ring resonator is relatively smaller than that for the ring-gap resonator, because the dielectric spacer below the ring-gap resonator has a small height, the conductor losses of the ground plane, excited by the gap fringing field, are high and are not included in calculations.

Figs. 7–9 show the field pattern of the first three non-leaky TE_{0pq} modes in a ring resonator, which has the ring sample shown in Fig. 6 with $s = 0$ and a smaller enclosure height $H = 6$ mm. The smaller H is selected so that the first three resonant modes are not leaky. The first resonant mode (TE_{011} mode) has the resonant frequency $f_r = 10.156$ GHz, the next (TE_{012} mode) $f_r = 17.444$ GHz and the third (TE_{021} mode) $f_r = 18.437$ GHz. All higher TE_{0pq} modes of this resonator are leaky modes, i.e., in the field solution equations (9) the $H_1^{(2)}$-functions (Hankel-functions) must be used in region $\rho > r_4 = 3.115$ mm.

The experiments show that the fundamental quasi-TE_{011} mode can be excited only if the gap in the sample is sufficiently small, e.g., $s < 400$ μm for the case of Fig. 6. The gap should be smaller if a higher order quasi-TE_{0pq} mode is excited. Furthermore the ring-gap resonator has the advantage that the fundamental quasi-TE_{011} mode can be excited dominantly suppressing other higher order modes at the same time. The best experimental result shows that no undesired modes can clearly be observed

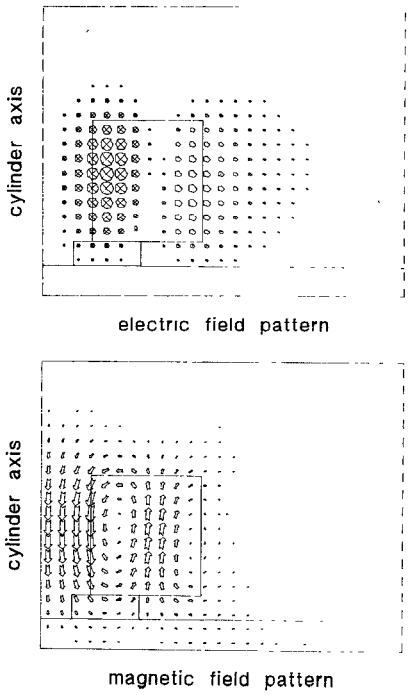

Fig. 9. Field pattern in a $\varphi = \text{const.}$ plane of the TE_{021} mode of the resonator of Fig. 7. Resonant frequency $f_r = 18.437$ GHz.

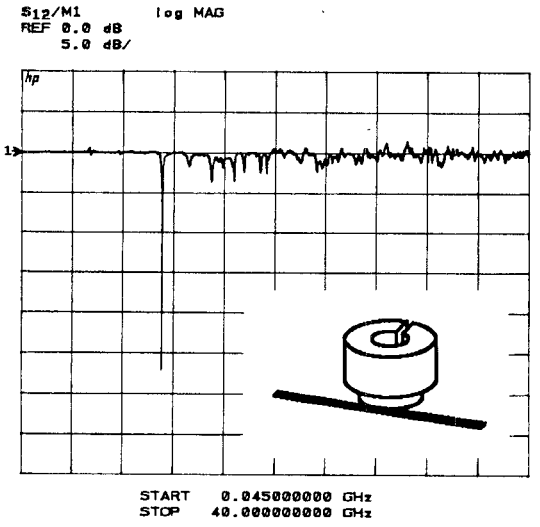

Fig. 10. Frequency responses of the dielectric ring-gap resonator excited by a nearby microstrip line.

over a measured frequency range from 45 MHz to 40 GHz, e.g., exciting the ring-gap resonator by a nearby microstrip, as shown in Fig. 10. This result has been carefully checked by repeating the same measurement in the sectional frequency ranges from 45 MHz to 40 GHz and by changing the position of the ring-gap sample azimuthally. If the same experiment is performed with a dielectric ring resonator, the higher order modes cannot be suppressed so effectively.

Other coupling techniques to couple the dielectric ring-gap resonator to e.g. a microstrip line on a thin substrate, using the electric fringing field near the gap edges, have been experimentally investigated and show promising

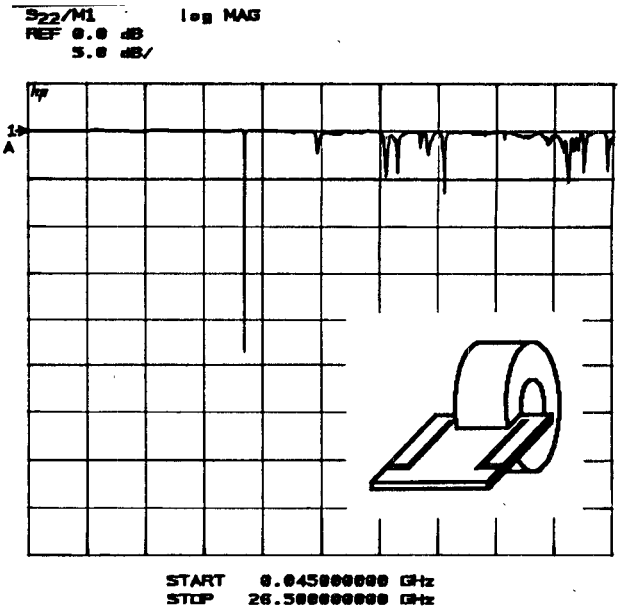

Fig. 11. Frequency response of the dielectric ring-gap resonator coupled to a microstrip line by the electric fringing field.

properties as shown in Fig. 11. The dielectric ring-gap resonator may also be coupled directly to a slotline or to a coplanar waveguide on the thin substrate by the electric fringing field. Using this coupling in MMIC's, for example in a MMIC oscillator [2], the circuits are more compact and bonding the MMIC chip onto a substrate can be avoided.

IV. Conclusion

Computer programs have been developed in *C* language to analyze and design a multicomposite multilayered cylindrical dielectric resonator and a dielectric ring-gap resonator. The characteristics of the fundamental quasi-TE_{011} mode in the ring-gap resonator have been theoretically and experimentally investigated. New coupling techniques to couple the ring-gap resonator to e.g., a microstrip line on a thin substrate, using the electric fringing field, have been experimentally investigated.

References

[1] D. Kajfez and P. Guillon, *Dielectric Resonators*. Norwood, MA: Artech House, 1984.

[2] S. B. Moghe and T. J. Holden, "High-performance GaAs MMIC oscillators," *IEEE Trans. Microwave Theory Tech.*, vol. MTT-35, no. 12, pp. 1283–1287, Dec. 1987.

[3] S. W. Chen and K. A. Zaki, "A novel coupling method for dual-mode dielectric resonators and waveguide filters," *IEEE Trans. Microwave Theory Tech.*, vol. 38, no. 12, pp. 1885–1893, Dec. 1990.

[4] Y. Kobayashi, N. Fukuoka, and S. Yoshida, "Resonant modes for a shielded dielectric rod resonator," *Electronics and Communications in Japan*, vol. 64-B, no. 11, pp. 46–51, 1981.

[5] U. Crombach and R. Michelfeit, "Resonanzfrequenzen und Feldstärken in geschirmten dielektrischen Scheiben- und Ringresonatoren", *Frequenz*, vol. 35, no. 12, pp. 324–328, 1981.

[6] S. Maj and M. Pospieszalshi, "A composite, multilayered cylindrical dielectric resonator," in *IEEE MTT-S Int. Microwave Symp. Dig.* 1984, pp. 190–192.

[7] U. Crombach, R. Gesche and N. Löchel, "Abstimmbare dielektrische Ringresonatoren," *Frequenz*, vol. 39, no. 1–2, pp. 45–49, 1985.

Wei Ke Hui was born in Qingdao, People's Republic of China, on August 13, 1957. He received the B.S. and M.S. degrees in electrical engineering from Northwest Telecommunications Engineering Institute (now named Xian Electrotechnical University), Xian, China, in 1982 and 1984, respectively. He is presently working on his Ph.D. thesis research in the area of theory of dielectric resonators and their applications in MMIC's in the Department of Electrical Engineering and Sondforschungsbereich 254, Duisburg University, Duisburg, Germany.

He was a Teaching Assistant from 1984 to 1986, and a Lecturer from 1986 to 1988 in the Department of Electromagnetic Field Engineering and Microwave Technique, Northwest Telecommunications Engineering Institute, where he taught courses on microwave techniques, microwave electronics and electromagnetic field theory, and pursued research in the area of dielectric resonators, dielectric resonator filters for application in MIC's, MIC DRO, low-noise MIC amplifiers, and MIC design techniques. Since 1988, he has been a Research Assistant in the Department of Electrical Engineering and Sondforschungsbereich 254, Duisburg University, where he is involved in research in the field of dielectric resonators for application in MMIC's.

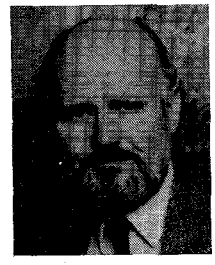

Ingo Wolff (M'75–SM'85–F'88) was born in Köslin, Germany, in 1938. He received the Dipl.-Ing., doctoral, and habilitation degrees in 1964, 1967, and 1970, respectively, all from the Technical University of Aachen, Germany.

From 1970 to 1974 he was a Lecturer and Associate Professor for high-frequency techniques in Aachen. Since 1974 he has been a Full Professor of Electromagnetic Field Theory at the University of Duisburg, Duisburg, Germany. His main areas of research are electromagnetic field theory applied to the computer-aided design of MIC's and MMIC's, millimeter-wave components and circuits, and the field theory of anisotropic materials.